





Weak signal extraction in non-stationary channel with weak measurement

Qi Song ^{1,4}, Hongjing Li ^{1,2,3,4}✉, Jingzheng Huang ^{1,2,3}, Peng Huang^{1,2,3}, Xiaorui Tan¹, Yu Tao¹, Chunhui Shi¹ & Guihua Zeng ^{1,2,3}✉

An emerging challenge of integrated communication and sensing is the extraction of weak sensing signals transmitted through an unknown non-stationary channel. In this work, we propose a weak signal extraction method with weak measurement. Taking advantage of time division multiplexing, we preliminarily estimate the channel via adjustable finite impulse response filter, further suppressing the interfering signal caused by background noises via spectrum shift. By subsequently using the time-varying phase estimation method via weak measurement, the real-time detection of weak signals in the non-stationary channel is achieved. We demonstrate via theoretical analysis and confirmatory experiment that our method is able to amplify the phase shift, to suppress technical noise and to improve detection resolution limit, while proving robust against light source fluctuations, initial phase differences and detector saturation. The method hence enables weak sensing signal extraction with a low signal-to-noise ratio non-stationary channel. Furthermore, we interface our measurement method to squeezed light sources, offering the possibility of surpassing standard quantum limit.

¹State Key Laboratory of Advanced Optical Communication Systems and Networks, Institute for Quantum Sensing and Information Processing, School of Sensing Science and Engineering, Shanghai Jiao Tong University, Shanghai 200240, P.R. China. ²Hefei National Laboratory, Hefei 230088, P.R. China.

³Shanghai Research Center for Quantum Sciences, Shanghai 201315, P.R. China. ⁴These authors contributed equally: Qi Song, Hongjing Li.

✉email: lhjnet2012@sjtu.edu.cn; ghzeng@sjtu.edu.cn

Recently, integrated communication and sensing (ICAS) have emerged as paradigm for developing applications in many fields, such as radar sensing system^{1–4}, distributed optical fiber sensing^{5–10}, internet of vehicles networks¹¹, quantum key distribution^{12–14}, etc. Its widespread applications not only require high communication performance, but also put forward higher requirements on the sensing precision and sensitivity. For example, a greater and finer seismic monitoring can be achieved by combining distributed optical fiber sensing technology with the existing communication optical cables^{9,10}. As another example, twin-field quantum key distribution (TF-QKD) can take advantage of redundancy information to obtain the vibration disturbance or temperature drift along the optical fiber link, which can locate the vibration disturbance¹⁴. Therefore, extracting sensing signal through communication channels, especially high precision identification of a weak signal with a low signal-to-noise ratio (SNR), becomes a potential challenge.

An accurate knowledge of the channel is the premise of signal extraction. As the channel is always changing with time in the actual environment, the non-stationary channel tracking should be considered, that is the channel must be re-estimated and updated progressively. The pilot-based channel estimation method has the advantages of low computational complexity and fast convergence, which is suitable for the real-time application of sensing signal transmission in a non-stationary channel^{3,4,15–17}. Furthermore, a high precision and sensitivity detection method is also essential to realize the identification of weak signals. Since weak measurement is derived in 1988¹⁸, it can amplify weak signal above technical noise^{19–23} interacted as the role of encoded parameter, including static parameter^{24–32} and time-varying parameter^{33–36}, which may provide a good solution for the task of the high sensitivity detection in practice.

In this paper, a weak signal extraction method with weak measurement is proposed, which can realize the extraction of weak sensing signal through a non-stationary channel for its capability on weak signal detection and noise suppression. The separation of interfering signal caused by channel background noises is implemented by using time-multiplexed preambles to estimate the channel via adjustable finite impulse response (FIR) filter and least mean square (LMS) criterion, while spectrum shift strategy can be adopted to further improve the SNR by modulating signal according to the estimation results. Meanwhile, weak measurement technique is applied to guarantee a real-time, sensitive and stable detection of the time-varying weak sensing signal. The weak sensing signal through the channel is encoded to a time-varying phase parameter and estimated by the change of light intensity. The method performs an enhancement in amplifying phase shift, suppressing technical noise and improving detection resolution limit, and it can also eliminate light source fluctuation, avoid detector saturation, has robustness in initial phase difference. When using squeezed state as light source, the method can surpass standard quantum limit (SQL). Moreover, a confirmatory experiment is designed, and the results showcase the method can realize the weak sensing signal extraction in a low SNR non-stationary channel. In potential, the insertion of reference phases enables a controllable sensitivity and linear dynamic range, and counteracts the influence of system initial phase absolutely. We believe the method could play a role towards the development of ICAS.

Results

Model setup. As shown in Fig. 1a, under the action of the signal source, each sensor in the ICAS network may obtain a sensing signal. The signal will be transmitted through a channel to the receiving end, which will be affected by different kinds of noises.

The actual channel always changes with time, and may exhibit non-stationary properties, that is, the noise power density spectrum of channel background noises is also time-varying. In some cases, the noises may be stronger than the sensing signal, which makes signal extraction more difficult. Here, we consider the transmission process of the sensing signal in the case that the interfering signal caused by the channel background noises is additive to the weak sensing signal.

In order to detect the weak sensing signal with high precision and sensitivity, a weak signal extraction method via weak measurement is proposed. As a general rule, we will denote scalar quantities by plain italics, vectors by boldface letters, the superscript “ H ” means transposition combined with complex conjugation and superscript “ $*$ ” means complex conjugation in the whole paper. Taking advantage of time division multiplexing, after sensing signal, each sensor sends the combination of preamble and sensing signal to receiving end through a non-stationary channel. Preambles are with labels, which can distinguish sensing signal and preamble of different sensors. It is worth noting that the length of preambles should be appropriate, too long will waste resources while too short could not get an efficient estimation of the channel. Channel pre-estimation can be performed to check whether the method can be applied, and determine the time fragmentation of preambles and the signal. One may refer to channel estimation method for details in the channel estimation part of methods section. In the subsequent analysis, we take a sensor as an example to show how the method is implemented.

In the receiving end, a weak signal detection system via weak measurement is designed to guarantee a high sensitivity and real time detection. As depicted in Fig. 1(b), the method performs preselection, weak interaction, and postselection on the prepared probe state, and measure the change of probe state. In the weak interaction process, the signal $x(t)$, including expected signal and interfering signal caused by unwanted channel background noises, is encoded into a time-varying phase parameter $\varphi(t)$. When detecting the change caused by the signal, it is necessary to consider the requirement of the selected probe state, and the real time detection requirement in practice, which needs a higher sampling rate.

After detection, adjustable FIR filter with LMS criterion is used to achieve channel estimation according to the information carried by preambles. As depicted in Fig. 1(c), preamble $p(t)$ through the channel is detected by weak measurement to form sampled signal $\mathbf{u}(\mathbf{n})$, as the input of the FIR filter with M taps. LMS criterion is used to adjust the tap weights according to the output of the comparator, that is the difference between the output of FIR filter $\hat{d}(n)$ and the desired response $d(n)$. Then a set of tap weights when the error is convergence can be obtained. Here, FIR filter is chosen to generate an output response to input data for its stability, which can guarantee the arbitrary amplitude-frequency characteristics while having strict linear phase-frequency characteristics, and easier to implement in hardware, which is suitable for real-time data processing. LMS criterion is chosen as the adaptive estimation mechanism, for it is efficient in the case that the prior knowledge of noises is limited^{37–40}.

Signal extraction can be realized according to the estimation results of each fragmentation. As a possible solution, the signal through the non-stationary channel can directly enter the FIR filter with the set of tap weights. For another possible solution, spectrum shift strategy can be adopted if the receiving end can send information to the sensors, then the method can escape strong interfering signal in a specific frequency band and estimation errors. According to the estimation results, the receiving end can obtain a power spectrum estimation of the

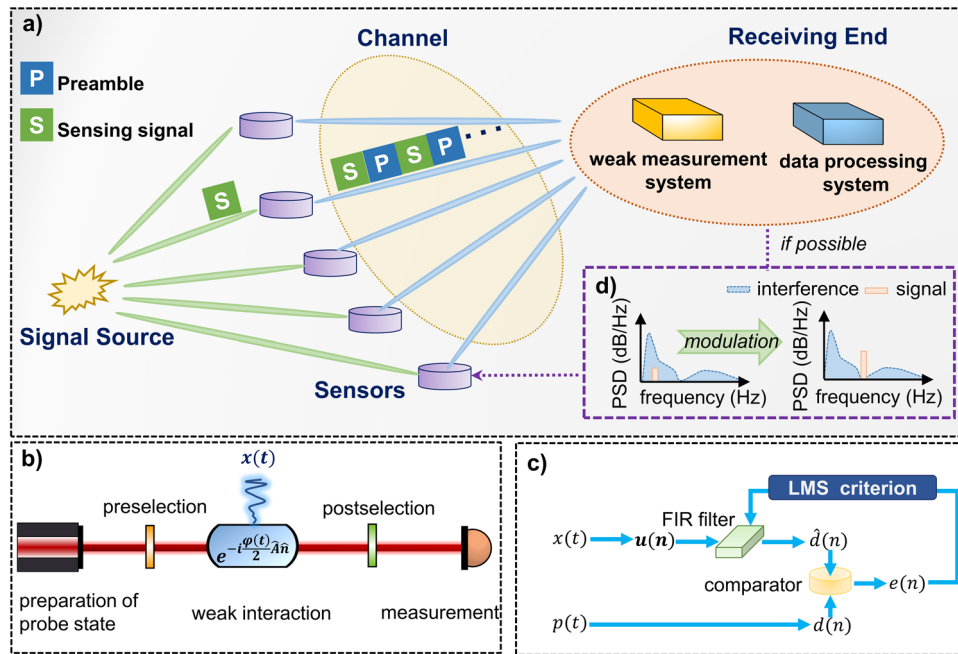


Fig. 1 The Schematic diagram of the weak signal extraction method with weak measurement. **a** A simple conceptual graph of the method. Each sensor in the integrated communication and sensing network obtains a sensing signal, and sends it to the receiving end with preambles through a changing non-stationary channel. In the receiving end, weak measurement system is used to guarantee a high sensitivity detection, while data processing system is used to realize channel estimation and signal extraction. **b** The schematic diagram of the high sensitivity time-varying phase estimation method via weak measurement. **c** The schematic diagram of channel estimation method via preamble and adjustable finite impulse response filter with least mean square criterion. **d** Effect of spectrum shift. With modulation, one can remove the signal to a low noise frequency band. Here, PSD stands for power spectral density.

background noises, figure out a low noise frequency band and inform the transmitter to shift the frequency spectrum of signal via modulation to escape from strong noises and achieve a better separation effect, as shown in Fig. 1d. Furthermore, the spectrum shift strategy is similar to frequency hopping communication, which may also resist multi-path fading and improve the security of communication⁴¹.

Weak signal detection via weak measurement. In this work, a weak signal detection method via weak measurement is proposed, as depicted in Fig. 1b. Our method uses weak measurement technique to amplify the phase shift introduced by time-varying signal, by coupling two physical systems, “system” and “pointer”, and reveals the phase shift by light intensity detection, which enables the detection of signals with higher frequency components and a relatively simple way to data processing. When light intensity is chosen as observable, the pointer is the photon number, and the photon number distribution will change in the measurement.

In the method, the preparation of pointer state can be adopted as the squeezed state, coherent state, classical light, etc. Here, we take coherent state as an example for analysis, which can be expressed as $|\alpha\rangle = \exp(-\frac{|\alpha|^2}{2}) \sum_n \frac{\alpha^n}{\sqrt{n!}} |n\rangle$, $|n\rangle$ denotes the Fock state with n photon number, and the mean photon number is $N = |\alpha|^2$.

In the preselection, the light beam is modulated as

$$|i\rangle = \frac{1}{\sqrt{2}}(|H\rangle + |V\rangle), \tag{1}$$

and the system-pointer joint state can be expressed as $|\Psi_i\rangle = |i\rangle|\alpha\rangle$. In the weak interaction process, a signal $x(t)$, including expected signal, or preambles, and the interfering signal caused by unwanted background noises, is encoded into a time-varying phase parameter $\varphi(t)$ between $|H\rangle$ and $|V\rangle$, the initial

state $|\Psi_i\rangle$ evolves to

$$|\Psi(t)\rangle = e^{-i\frac{\varphi(t)}{2}\hat{A}\hat{n}}|i\rangle|\alpha\rangle, \tag{2}$$

where the Stokes polarization operator $\hat{A} = |H\rangle\langle H| - |V\rangle\langle V|$ acts on the system, and the photon number operator $\hat{n} = \hat{a}^\dagger\hat{a}$ acts on the pointer. Here, \hat{a} is annihilation operator and \hat{a}^\dagger is creation operator. In the postselection process, the evolved state $|\Psi(t)\rangle$ is projected to final state

$$|f\rangle = \frac{1}{\sqrt{2}}(ie^{i\varepsilon}|H\rangle - ie^{-i\varepsilon}|V\rangle), \tag{3}$$

which is nearly orthogonal to the preselection with a postselection angle $\varepsilon \ll 1$ for a high amplification factor.

After postselection, the final pointer state can be written as

$$\begin{aligned} |p_f(t)\rangle &= \langle f|e^{-i\frac{\varphi(t)}{2}\hat{A}\hat{n}}|i\rangle|\alpha\rangle \\ &= \frac{-ie^{-i\varepsilon}}{2}|\alpha e^{-i\frac{\varphi(t)}{2}}\rangle + \frac{ie^{i\varepsilon}}{2}|\alpha e^{i\frac{\varphi(t)}{2}}\rangle. \end{aligned} \tag{4}$$

The average photon number for the final state is associated with possibility⁴², i.e.,

$$\langle n \rangle = |\alpha|^2 \sin^2[\varepsilon + \frac{\varphi(t)}{2}], \tag{5}$$

and the output light intensity can be expressed as

$$I_1(t) = I_0(t) \sin^2[\varepsilon + \frac{\varphi(t)}{2}], \tag{6}$$

where $I_0(t)$ denotes initial light intensity of the source.

Under the condition of $|ImA_w\varphi(t)/2| \ll 1$, where A_w is so-called weak value, i.e.

$$ImA_w = Im \frac{\langle f|\hat{A}|i\rangle}{\langle f|i\rangle} = \cot \varepsilon, \tag{7}$$

the final pointer state can be expressed as

$$|p_f(t)\rangle = \langle f|i\rangle e^{-i\frac{\varphi(t)}{2}A_w\hat{n}}|\alpha\rangle. \tag{8}$$

Correspondingly, Eq. (6) can be approximated to

$$\begin{aligned} I_1(t) &\approx I_0(t)\sin^2\varepsilon[1 + \varphi(t)ImA_w] \\ &\approx I_0(t)\varepsilon^2 + I_0(t)\varepsilon\varphi(t). \end{aligned} \tag{9}$$

When no signal inputs, the output light intensity is $I_i(t) = I_0(t)\sin^2\varepsilon \approx I_0(t)\varepsilon^2$, and the unknown time-varying phase shift $\varphi(t)$ can be obtained by the change of $I(t)$ before and after signal input, i.e.,

$$\begin{aligned} \Delta I_1(t) &= I_1(t) - I_i(t) \\ &= I_0(t)\varepsilon\varphi(t). \end{aligned} \tag{10}$$

Quantified performance advantage. First, we focus on the quantified advantage of the method in phase shift estimation. In order to illustrate the advantage, a comparison with standard interference technique is made. For standard interference technique, a equivalent interferometer similar to the equivalence by Brunner and Simon²⁸ is designed. The light is polarized at 45° , $\frac{1}{\sqrt{2}}(|H\rangle + |V\rangle)$, also introduced a time-varying phase $\varphi(t)$ between $|H\rangle$ and $|V\rangle$, and then operated in a circular polarization $\frac{1}{\sqrt{2}}(|H\rangle + i|V\rangle)$. When $|\varphi(t)| \ll 1$ is weak, the out intensity is

$$\begin{aligned} I_s(t) &= \frac{I_0(t)}{2}[1 + \sin\varphi(t)] \\ &\approx \frac{I_0(t)}{2}[1 + \varphi(t)], \end{aligned} \tag{11}$$

and the change in light intensity is

$$\begin{aligned} \Delta I_s(t) &= \frac{I_0(t)}{2}\sin\varphi(t) \\ &\approx \frac{I_0(t)}{2}\varphi(t). \end{aligned} \tag{12}$$

Compared the method and the equivalent interferometer from Eqs. (9) and (11), the method has an attenuation factor of $2\varepsilon^2$ in the detected light intensity, but only an attenuation factor of 2ε in the phase shift, the phase shift is actually amplified with a factor

of $1/\varepsilon$. In order to show the amplification effect more intuitively, the change in light intensity relative to the initial is used as the indicator, as shown in Fig. 2a. As a result, the system works in a thinner linear dynamic range and has a higher amplification factor when setting a smaller postselection angle. Furthermore, as the detected light intensity is highly attenuated, the method can effectively avoid detector saturation, and a low-saturation can be used. Indeed, the attenuation of the detected light intensity reflects the requirements for detection devices, detectors with high resolution and low minimum detectable intensity or amplifiers can solve this problem well.

In practice, the measurement system suffers some technical issues, which will affect the actual precision. Then we consider two types of them, the noise related to light intensity or photon number and alignment error, and show that the method can outperform equivalent interferometer in the presence of these issues.

The noise related to light intensity or photon number, which can be expressed as $I_N(t) = \delta I_0(t)$, such as relative intensity noise, thermal noise^{19,32,43}. SNR is chosen as figure of merit to measure the enhancement of the method. The equivalent interferometer has a SNR of

$$\begin{aligned} SNR_s &= \frac{\Delta I_s(t)}{\delta I_s(t)} \\ &= \frac{\frac{I_0(t)}{2}\varphi(t)}{\frac{I_0(t)}{2}\delta[1 + \sin\varphi(t)]} \\ &\approx \frac{\varphi(t)}{\delta}, \end{aligned} \tag{13}$$

and the method has a SNR of

$$\begin{aligned} SNR_w &= \frac{\Delta I(t)}{\delta I(t)} \\ &= \frac{I_0(t)\sin^2[\varepsilon + \frac{\varphi(t)}{2}] - I_0(t)\sin^2(\varepsilon)}{I_0(t)\delta\sin^2[\varepsilon + \frac{\varphi(t)}{2}]} \\ &\approx \frac{1}{\varepsilon} \frac{\varphi(t)}{\delta}. \end{aligned} \tag{14}$$

Thus, the method has an improvement of SNR of $1/\varepsilon$ on the noise related to light intensity or photon number, as shown in Fig. 2b.

The transmittance rate of optical devices is impossible to be 100%, and there may be a difference γ between $|H\rangle$ and $|V\rangle$ ²³. Then alignment error occurs, which deviates the splitting ratio of $|H\rangle$ and $|V\rangle$ from 1:1 to $(1+\gamma/2):(1-\gamma/2)$, leads a potentially erroneous detection of detector, and restricts the detection resolution limit to the detection method^{28,43}. For the equivalent interferometer, $(I_0(t)/2)\varphi(t) > I_0(t)\gamma$ should be satisfied, and the detection resolution limit is $\varphi(t) > 2\gamma$. Meanwhile, the detection resolution limit is in the method is $\varphi(t) > \varepsilon\gamma$, given by $I_0(t)\varepsilon\varphi(t) > I_0(t)\varepsilon^2\gamma$. Therefore, the method also leads an improvement of $2/\varepsilon$ in detection resolution limit.

Finally, an analysis of the precision of the method is carried out. Under the condition of $|ImA_w\varphi(t)/2| \ll 1$, the final pointer state can be normalized as

$$|p_f(t)\rangle = e^{-i\frac{\varphi(t)}{2}A_w\hat{n}}|\alpha\rangle, \tag{15}$$

and the obtained possibility of the pure $\varphi(t)$ -based state, $|p_f(t)\rangle$ can be approximated to $p = |\langle f|i\rangle|^2 = \sin^2\varepsilon$. The quantum

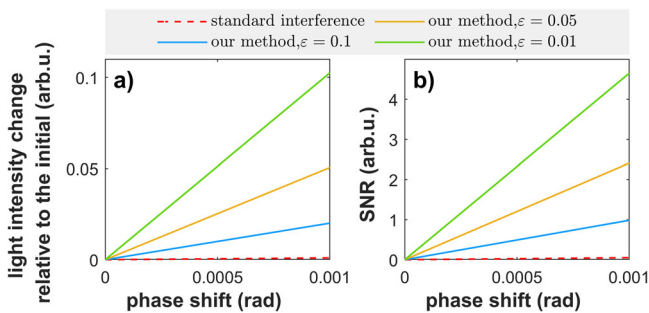


Fig. 2 The comparison with equivalent interferometer and the method under different postselection angles. **a** The amplification effect of the phase shift according to the change in light intensity relative to the initial. **b** The SNR of technical noise related to light intensity or photon number. Here, the red dashed line stands for standard interference, and the blue, yellow, and green line reflects our method when setting postselection angle as 0.1, 0.05, and 0.01, respectively.

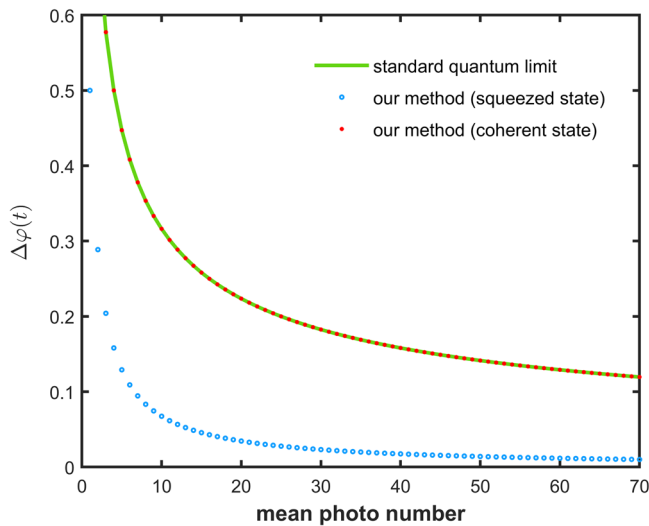


Fig. 3 Standard deviation of $\varphi(t)$ obtained when using coherent state and squeezed state. The green line showcases the standard quantum limit. Red points show the standard deviation of $\varphi(t)$ when using coherent state as light source, and blue circles show that by using the optimal Gaussian state.

Fisher information (QFI) of $|p_f(t)\rangle$ can be expressed as

$$\begin{aligned}
 Q(t) &= 4\text{Re} \left(\frac{\partial \langle p_f(t) |}{\partial \varphi(t)} \right) \left(\frac{\partial |p_f(t)\rangle}{\partial \varphi(t)} \right) \\
 &\quad - 4\text{Re} \left(\frac{\partial \langle p_f(t) |}{\partial \varphi(t)} \right) |p_f(t)\rangle \langle p_f(t)| \left(\frac{\partial |p_f(t)\rangle}{\partial \varphi(t)} \right) \quad (16) \\
 &= |A_w|^2 (\langle n^2 \rangle - \langle n \rangle^2) \\
 &= |A_w|^2 (\Delta n)^2,
 \end{aligned}$$

and the total QFI of the method can be expressed as

$$F(t) = pQ(t) = \cos^2 \varepsilon (\Delta n)^2, \quad (17)$$

which indicates that the precision limit of each measurement is related to the variance of photon number, $(\Delta n)^2$ ^{42,44,45}. When using coherent state as the light source, $(\Delta n)^2 = N$, and the total QFI is $\cos^2 \varepsilon N$. The standard deviation of $\varphi(t)$, $\Delta \varphi(t)$ is in the scaling of $1/\sqrt{N}$, which can approach SQL, as shown in Fig. 3.

Using squeezed state as the light source can further enhance the sensitivity and precision, which has been demonstrated in many applications, such as gravitational wave detection^{46,47}. For squeezed state, one can apply a squeezing along a fixed direction $S(r) = \exp((r/2)(\hat{a}^2 - \hat{a}^{\dagger 2}))$, where r is the compression parameter, and a displacement $D(\alpha) = \exp(\alpha \hat{a}^\dagger - \alpha^* \hat{a})$ on vacuum state $|0\rangle$. When employing all available energy in squeezing the vacuum state can achieve the highest sensitivity, which is so-called the optimal Gaussian state⁴⁸. When the optimal Gaussian state is applied to the method as light source, $(\Delta n)^2 = 2(n_r^2 + n_r)$, where $n_r = \sinh^2 r$ is the mean photon number^{48–50}, here, $\Delta n > n_r$, which does not satisfy the condition of the form of Heisenberg limit of $1/n_r$ by Ou^{51,52}. In this case, the total QFI is $2\cos^2 \varepsilon (n_r^2 + n_r)$, $\Delta \varphi(t)$ is in the scaling of $1/\sqrt{n_r^2 + n_r}$, and the method can surpass SQL, as shown in Fig. 3.

Experimental verification. In our method, the total noises can be divided into two parts, the interfering signal caused by unwanted background noises and the technical noise caused by detecting the weak signal. As discussed above, the weak signal detection

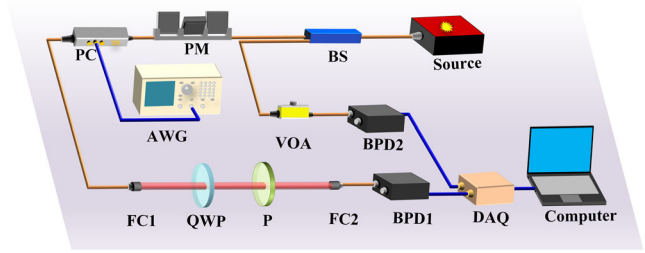


Fig. 4 Schematic diagram of the experimental setup. Here, the orange line is the optical fiber, blue line is electric wire and red line is the light beam in free space. BS beam splitter, PC polarization controller, PM phase modulator, AWG Arbitrary waveform generator, VOA variable optical attenuator, FC1, FC2 fiber collimator, QWP quarter wave plate, P polarizer, BPD1 BPD2, balanced photoelectric detector, DAQ Data Acquisition Card.

method via weak measurement can realize the estimation of phase shift and suppress the technical noise. However, the interfering signal caused by unwanted background noises combines with the sensing signal in the transmission of sensing signal through the non-stationary channel and encode into the weak measurement system. Extracting the expected signal from the phase shift is a significant part in ICAS, it is necessary to consider channel estimation, which is realized via the preambles and FIR filter with LMS criterion.

As depicted in Fig. 4, a confirmatory experiment is designed to showcase the channel estimation effect of the method. In the theoretical analysis, we have shown the performance advantages and quantum enhancement when using squeezed state, and the performance advantages of phase shift amplification, the SNR improvement, and detection resolution limit improvement are also established in classical light sources. For practical application considerations, we use a classical light to perform the experiment, a single frequency laser is chosen as the light source. In practice, the light source may fluctuate due to changes in parameters such as temperature, electric current, etc. To solve this problem, the light beam is split into two paths where the 1st path is used to detect the signal, and the 2nd path is used to monitor the light source. The light split ratio between the 1st path and the 2st path are $\eta_1: \eta_2 = \eta$, and it can be processed with $R(t)$, i.e. $R(t) = \frac{I_s(t)}{I_0(t)} \approx \eta \varepsilon^2 + \eta \varepsilon \varphi(t)$. The unknown time-varying phase shift can be also obtained by the change of $R(t)$ without light intensity fluctuation, $\Delta R(t) = R(t) - R_0(t) = \eta \varepsilon \varphi(t)$. In addition, a microcontroller or field programmable gate array can replace the data acquisition card and computer for the requirement of real-time processing in practical engineering. One may refer to experimental materials and calibration for details in the methods section.

In experimental setup, we choose sinusoidal signal with single frequency as preamble, and perform two groups of experiment with a sampling frequency of 100kHz. The amplitude and frequency of sinusoidal preamble are 500mV and 100Hz in Group 1, while the amplitude and frequency of sinusoidal preamble are 50mV and 400Hz in Group 2. For the interfering signal caused by unwanted background noise, as pulse noise under Gaussian mixture noise exist in many scenarios, such as, marine ambient noise of Arctic Ocean⁵³, short-wave broadband channel⁵⁴, etc., we choose the consist of pulse noise under Gaussian mixture noise as the channel background noise. Moreover, the detection results also contain technical noise, such as electrical noise and imperfection of different devices, etc. Due to the technical noise and the filtering effect of balanced photoelectric detector, the actual noises are more complex than the preset channel background noises.

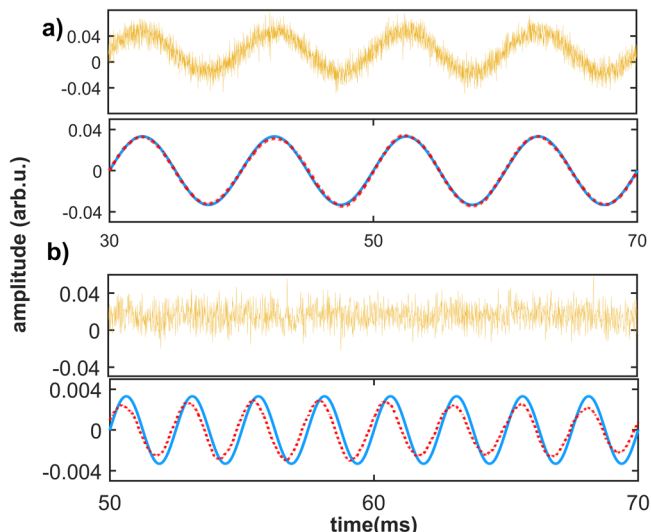


Fig. 5 The fragment of the 100ms preamble recovery results. **a** The recovery results of Group 1. **b** The recovery results of Group 2. Here, the yellow lines are the measured values of each group, while the blue lines are the desired response of FIR, and the red dotted lines are the actual response of the FIR filter. In the vertical coordinate, the amplitude is $k\varphi$, where k is a constant, one may refer to experimental materials and calibration for details in the methods section.

Table 1 Figure of merit of the recovery results.

Group ^a	1	2
SNR before processing	2.1032dB	-18.1594dB
SNR after processing	28.8022dB	8.1715dB
the improvement of SNR	26.6991dB	26.3309dB
root-mean-square error	8.5534×10^{-4}	9.1597×10^{-4}
mean absolute error	7.1272×10^{-4}	7.7293×10^{-4}

^aThe two groups of experiment results are different sinusoidal preambles through the non-stationary channel with pulse noise under Gaussian mixture noise with a sampling frequency of 100kHz. The amplitude and frequency of Group 1 and Group 2 are 500mV and 100Hz, 50mV and 400Hz, respectively.

According to the convergence situation, a set of the tap weights is chosen to estimate the channel. One may refer to channel estimation method for details in the methods section. In order to intuitively display the noises separation effect of the method, we first recover the preamble. As shown in Fig. 5, the estimated values are in good agreement with the desired response. Root-mean-square error, mean absolute error and the improvement of SNR are further chosen as the figure of merit to quantitatively measure errors and the improvement of SNR. As listed in Table 1, the results show that the improvement of SNR can reach 26dB, which suggests the feasibility that a set of the tap weights when convergence can extract the signal well.

As shown in Fig. 1d, frequency spectrum shift strategy could be used in the method. Thus, an estimation of noise frequency spectrum is essential, the results is depicted in Fig. 6. The method has a great estimation result from Fig. 6a, c. In the process of detection by photodetector, electrical noise will disturb the detection results. As the noises in low frequency range is more complicated⁵⁵, we further explore the noise frequency spectrum estimation in the frequency lower than 2 kHz. As shown in Fig. 6b, d, the method also has a good result, although only a few frequencies are not accurately estimated. Overall, the estimation results verify the feasibility of the method in a low-SNR non-

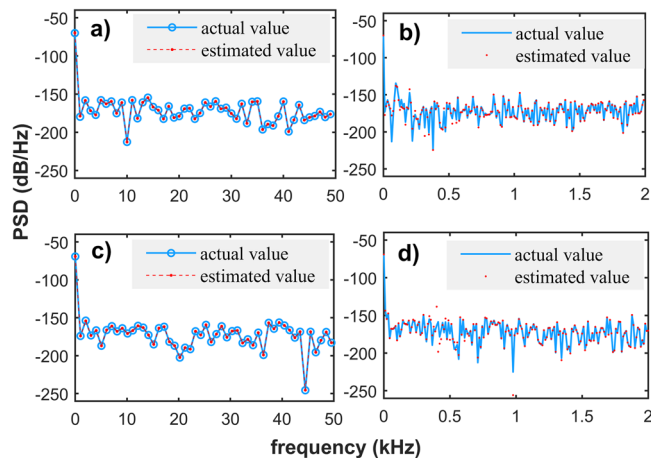


Fig. 6 Noise power spectrum density estimation results. **a** The overall noise power spectrum density estimation of Group 1. **b** The noise power spectrum density estimation in the range of lower than 2 kHz of Group 1. **c** The overall noise power spectrum density estimation of Group 2. **d** The noise power spectrum density estimation in the range of lower than 2 kHz of Group 2. In a and c, the blue line with circles shows the actual values, and red dashed line with points shows the estimation values. In b and d, the blue line shows the actual values, and red points show the estimation values. Here, the results are also calculated by $k\varphi$, and PSD stands for power spectral density.

stationary channel with pulse noise under Gaussian mixture noise, which lays the foundation for ensuring the spectrum shifting strategy.

Discussion

In summary, a signal extraction method with weak measurement is proposed and experimentally demonstrated to extract weak sensing signal through an unknown non-stationary channel. The method performs enhancement in detecting weak signal, which enables a real-time, sensitive and stable detection. With time division multiplexing, preambles are designed to realize the noise estimation in the non-stationary channel via adjustable FIR filter with LMS criterion. According to the results, weak sensing signal can be identified, and spectrum shift strategy can be used to further improve the SNR via signal modulation if conditions permit. Moreover, a confirmatory experiment is performed, and the results illustrate the feasibility of the method in a low-SNR non-stationary channel with pulse noise under Gaussian mixture noise. The method may provide a good solution in the difficult and potential task of weak sensing signal extraction under the trend of ICAS.

In the weak signal detection of the method, weak measurement technique performs quantum operation on photonics by setting the postselection state which is nearly orthogonal to the pre-selection state at the cost of light attenuation loss. Compared with standard interference technique, the method has an amplification in the phase shift with a factor of $1/\epsilon$, an improvement of SNR of $1/\epsilon$ on the noise or error related to light intensity or photon number, and an improvement of detection resolution limit of $2/\epsilon$ in the ideal case. The light attenuation loss can avoid detector saturation, although it puts forward higher requirement for the minimum detectable intensity and resolution of detectors and data acquisition equipment. When using squeezed light as light source, the method may offer the possibility of surpassing SQL.

When the method is applied into the practice, there may be an initial phase difference φ_0 between $|H\rangle$ and $|V\rangle$, which is also non-negligible in experimental setup. Still under the condition of

$|\frac{\varphi(t)}{2}ImA_w| \ll 1$, $ImA_w = \cot(\varepsilon + \varphi_0/2)$, $\Delta R(t)$ can be rewritten as $\Delta R(t) \approx \eta \sin^2(\varepsilon + \frac{\varphi_0}{2})\varphi(t)ImA_w$, and correspondingly, the amplification factor in the phase shift will reduce to $\cot(\varepsilon + \varphi_0/2)$, and the improvement of SNR on the noise or error related to light intensity or photon number will also reduce to $\cot(\varepsilon + \varphi_0/2)$. Thus, the existence of the initial phase difference φ_0 may lead to an unsatisfactory amplification factor. In order to solve this problem, an adaptive adjustment strategy can be utilized by adjusting postselection angle ε ⁵⁶ or inserting a reference phase in the 1st path^{34,36,57}. The adaptive adjustment strategy can guarantee the amplitude of an unknown time-varying parameter always meets the weak measurement condition in practical application, even the initial phase difference φ_0 is time-varying, and enables the method a controllable sensitive and linear dynamic range.

Furthermore, in the practical application, the light intensity may exist large fluctuation, not like the case in the experiment that the light intensity can be considered to almost non-fluctuation. Due to a time delay exists between the signal path and light intensity monitoring path, a synchronizer is needed. One possible solution is modulating the light source with pulses as synchronization markers.

Methods

Channel estimation method. In the method, channel estimation is realized via preambles and FIR filter with LMS criterion. As shown in Fig. 1c, the preamble $p(t)$ through the non-stationary complicated channel is detected by weak measurement system, and get the sampled signal $\mathbf{u}(\mathbf{n})$, which is processed by a FIR filter with M taps. We denote the input of the FIR filter at any moment as a $M \times 1$ tap input vector $\mathbf{u}(\mathbf{n}) = \{u(n), u(n-1), \dots, u(n-M+1)\}$, while the tap weights of the FIR filter is denoted as a $M \times 1$ tap weights vector, $\hat{\mathbf{w}}(\mathbf{n}) = \{\hat{w}_0(n), \hat{w}_1(n), \dots, \hat{w}_{M-1}(n)\}$. Then the output of FIR filter is

$$\hat{d}(n) = \hat{\mathbf{w}}^H(\mathbf{n})\mathbf{u}(\mathbf{n}), \quad (18)$$

which is the estimation of the desired response $d(n)$, the sampling sequence of a time-delayed preamble. The comparator is used to compare $\hat{d}(n)$ and $d(n)$, and its output is the estimation error, i.e.

$$e(n) = \hat{d}(n) - d(n), \quad (19)$$

which is used to adjust the tap weights $\hat{\mathbf{w}}(\mathbf{n} + 1)$ according to the LMS criterion.

In order to track the change of channel, a cost function is defined,

$$J(n) = |e(n)|^2 = e(n)e^*(n) \quad (20)$$

to adapt to statistical variations of the unknown channel. According to the LMS criterion, the updated tap-weight vector $\hat{\mathbf{w}}(\mathbf{n} + 1)$ is optimal in the meaning of mean square error⁴⁰, and the updating rule is

$$\hat{\mathbf{w}}(\mathbf{n} + 1) = \hat{\mathbf{w}}(\mathbf{n}) + \mu\mathbf{u}(\mathbf{n})e^*(n) \quad (21)$$

where μ is step-size parameter, and a larger μ has a faster convergence rate. It is emphasized that μ is a relatively small positive value, which should satisfy $0 < \frac{1}{2}\mu\|\mathbf{u}(\mathbf{n})\|^2 < 1$, where $\|\mathbf{u}(\mathbf{n})\|^2$ is the squared Euclidean norm of the input vector $\mathbf{u}(\mathbf{n})$. The tap-weight vector at the time of convergence can be denoted as $\mathbf{w}(\mathbf{n})$.

In fact, the FIR output error is minimized to achieve convergence by adjusting the convergence is determined by the taps of FIR M and the step-size parameter of LMS criterion μ . In the experiment, The convergence situation of Group 1 is shown in Fig. 7a, the taps of the FIR is $M = 500$, and the step-size parameter of LMS criterion is $\mu = 0.005$. The convergence

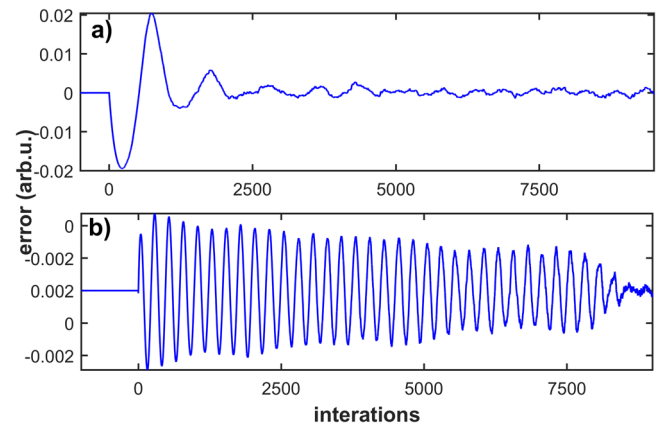


Fig. 7 Convergence situation. **a** Convergence situation of Group1, the taps of finite impulse response is $M = 500$, and the step-size parameter of least mean square criterion is $\mu = 0.005$. **b** Convergence situation of Group2, the taps of finite impulse response is $M = 1000$, and the step-size parameter of least mean square criterion is $\mu = 0.05$. In the vertical coordinate, the error is the amplitude error of $k\varphi$.

situation of Group 2 is shown in Fig. 7b, the taps of the FIR is $M = 1000$, and the step-size parameter of LMS criterion is $\mu = 0.05$. By comparing the convergence situation, a lower SNR needs more convergence time, which needs increasing the length of preamble fragmentation and more taps, which reflects the requirements on computational performance and hardware structure in practice.

Indeed, the method expects the tap weights vector $\mathbf{w}(\mathbf{n})$ can be converged when estimating channel via the preamble, and the convergence can be sustainable when the signal is received. Thus misadjustment M_a is defined to measure whether $J(n)$ can be accepted, i.e.

$$M_a(n) = \frac{J_{ex}(n)}{J_{min}}, \quad (22)$$

where J_{min} is the mean square error at time of convergence, and $J_{ex}(n) = J(n) - J_{min}$ is real-time value of the excess mean square error. Eq. (22) can be expressed as

$$M_a(n) = \frac{1}{2}\mu\|\mathbf{u}(\mathbf{n})\|^2 \quad (23)$$

when μ is small. Usually, M_a is often smaller than 10% in practical application⁴⁰.

Experimental materials and calibration. The schematic diagram of the experimental setup, is shown in Fig. 3. The light beam emits from a single frequency laser (NLFL-1550-50-SM-M) with a central wavelength of 1550 nm, and is split into two paths through a fiber beam splitter (TW1550R5A1, Thorlabs). In the first path, the light beam is collected by a fiber collimator (60FC-4-A11-45, Schäfer+Kirchhoff) and enters a polarization controller (FPC032, Thorlabs) to preselect the polarization state. Then the light passes through a phase modulator (LN53S-FC, Thorlabs), which encodes the simulated signals passing through a complicated channel generated by an arbitrary waveform generators (AFG3011C, Tektronix) into time-varying phase parameter. After that, the output light passes through a quarter-wave plate (AQWP10M-1600, Thorlabs) and a polarizer (LPNIR100-MP2, Thorlabs), which play the role of postselection, and the intensity was collected by a fiber collimator and monitored by the first balanced photoelectric detector (PDB440C, Thorlabs). In the second path, the light beam is attenuated by a variant optical attenuator, which avoids detection equipment damage caused by

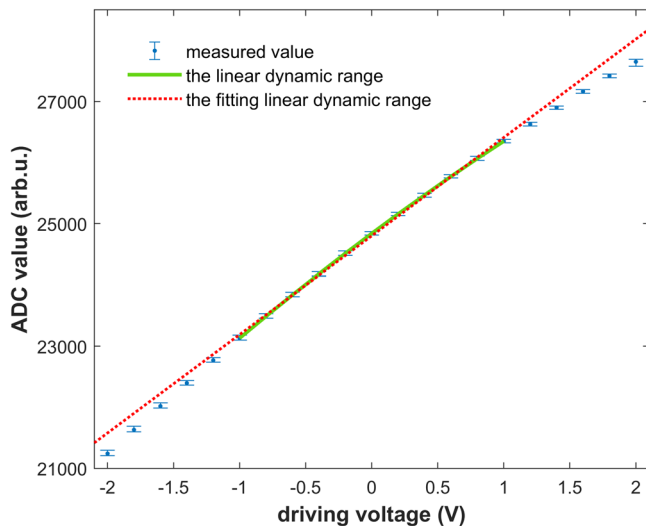


Fig. 8 The analog-to-digital conversion values of the 1st path detected by weak measurement under different driving voltages and the calibration results. The blue points show the average measured values of 500 measurements, and the error bars showcase the maximum and minimum values. The green line labels the linear dynamic range, and the red dotted line shows the fitting results with a correlation coefficient of 0.9988. Here, ADC value is analog-to-digital conversion value.

excessive light and then collected by the second balanced photoelectric detector. Finally, the detection data of two balanced photoelectric detectors are processed by a data acquisition card (S Bench6, Spectrum) with a 16-bit analog-to-digital converter (ADC) and a sampling frequency of 100kHz and a computer.

In the experiment setup, the phase introduced by phase modulator has a linear relation with its driving voltage in the range of its half wave voltage, about from -7V to 7V. As the light intensity monitored by the 2nd path is almost stable with an average ADC value of 24155 after attenuating about 40dB by the variant optical attenuator, we choose the driving voltage as the independent variable and the ADC values of the 1st path as the dependent variable to calibrate, as depicted in Fig. 8. The fitting linear dynamic range can be expressed as $I_1 = 1610x + 24800$, with a correlation coefficient of 0.9988, where x is driving voltage of the phase modulator.

Above all, as the phase introduced by phase modulator has a linear relation with its driving voltage, and I_1/I_2 also has a linear relation with the driving voltage, the unknown time-varying phase is in direct proportion to the change of I_1/I_2 , i.e. $(I_1(t) - 24800)/I_2(t) = k\varphi(t)$. Therefore, we collect the light intensity of the 1st path and the 2nd path, and take $(I_1 - 24800)/I_2$ as the input of FIR in data processing.

Data availability

All data needed to evaluate the conclusions in the paper are preset in the paper. Additional data related to this paper are available from the corresponding author upon reasonable request.

Code availability

The computer codes that support the findings presented in the main text are available from the corresponding author upon reasonable request.

Received: 5 May 2023; Accepted: 4 December 2023;

Published online: 21 December 2023

References

- Zhang, J. A. et al. An overview of signal processing techniques for joint communication and radar sensing. *IEEE J. Sel. Top. Signal Process.* **15**, 1295–1315 (2021).
- Amin, M. G., Zhang, Y. D., Ahmad, F. & Ho, K. D. Radar signal processing for elderly fall detection: The future for in-home monitoring. *IEEE Signal Process. Mag.* **33**, 71–80 (2016).
- Kumari, P., Choi, J., González-Prelcic, N. & Heath, R. W. Ieee 802.11ad-based radar: An approach to joint vehicular communication-radar system. *IEEE Trans. Vehicular Technol.* **67**, 3012–3027 (2018).
- Barneto, C. B., Liyanaarachchi, S. D., Heino, M., Riihonen, T. & Valkama, M. Full duplex radio/radar technology: The enabler for advanced joint communication and sensing. *IEEE Wirel. Commun.* **28**, 82–88 (2021).
- Yan, Y. et al. Distributed optical fiber sensing assisted by optical communication techniques. *J. Lightwave Technol.* **39**, 3654–3670 (2021).
- Lindsey, N. J. et al. Fiber-optic network observations of earthquake wavefields. *Geophys. Res. Lett.* **44**, 11–792 (2017).
- Lindsey, N. J., Dawe, T. C. & Ajo-Franklin, J. B. Illuminating seafloor faults and ocean dynamics with dark fiber distributed acoustic sensing. *Science* **366**, 1103–1107 (2019).
- Catalano, E. et al. Automatic traffic monitoring by ϕ -otdr data and hough transform in a real-field environment. *Appl. Opt.* **60**, 3579–3584 (2021).
- Li, Z. et al. Rapid response to the 2019 ridgecrest earthquake with distributed acoustic sensing. *AGU Adv.* **2**, e2021AV000395 (2021).
- Jousset, P. et al. Dynamic strain determination using fibre-optic cables allows imaging of seismological and structural features. *Nat. Commun.* **9**, 2509 (2018).
- Siegel, J. E., Erb, D. C. & Sarma, S. E. A survey of the connected vehicle landscape-architectures, enabling technologies, applications, and development areas. *IEEE Trans. Intell. Transp. Syst.* **19**, 2391–2406 (2017).
- Weedbrook, C. et al. Gaussian quantum information. *Rev. Mod. Phys.* **84**, 621–669 (2012).
- Xu, F., Ma, X., Zhang, Q., Lo, H.-K. & Pan, J.-W. Secure quantum key distribution with realistic devices. *Rev. Mod. Phys.* **92**, 025002 (2020).
- Chen, J.-P. et al. Quantum key distribution over 658 km fiber with distributed vibration sensing. *Phys. Rev. Lett.* **128**, 180502 (2022).
- Wu, Q., Zhou, X., Wang, C. & Qin, Z. Channel estimation based on superimposed pilot and weighted averaging. *Sci. Rep.* **12**, 1–15 (2022).
- Şenol, H. & Tepedelenlioğlu, C. Subspace-based estimation of rapidly varying mobile channels for ofdm systems. *IEEE Trans. Signal Process.* **69**, 385–400 (2021).
- Abdazadeh-Ziabari, H., Zhu, W.-P. & Swamy, M. N. S. Joint carrier frequency offset and doubly selective channel estimation for mimo-ofdma uplink with kalman and particle filtering. *IEEE Trans. Signal Process.* **66**, 4001–4012 (2018).
- Aharonov, Y., Albert, D. Z. & Vaidman, L. How the result of a measurement of a component of the spin of a spin-1/2 particle can turn out to be 100. *Phys. Rev. Lett.* **60**, 1351 (1988).
- Jordan, A. N., Martínez-Rincón, J. & Howell, J. C. Technical advantages for weak-value amplification: when less is more. *Phys. Rev. X* **4**, 011031 (2014).
- Starling, D. J., Dixon, P. B., Jordan, A. N. & Howell, J. C. Optimizing the signal-to-noise ratio of a beam-deflection measurement with interferometric weak values. *Phys. Rev. A* **80**, 041803 (2009).
- Ma, F.-Y., Li, J.-G. & Zou, J. The influence of non-gaussian noise on weak values. *Phys. Lett. A* **388**, 127027 (2021).
- Feizpour, A., Xing, X. & Steinberg, A. M. Amplifying single-photon nonlinearity using weak measurements. *Phys. Rev. Lett.* **107**, 133603 (2011).
- Fang, C., Huang, J.-Z. & Zeng, G. Robust interferometry against imperfections based on weak value amplification. *Phys. Rev. A* **97**, 063818 (2018).
- Dressel, J., Malik, M., Miatto, F. M., Jordan, A. N. & Boyd, R. W. Colloquium: Understanding quantum weak values: Basics and applications. *Rev. Mod. Phys.* **86**, 307 (2014).
- Hosten, O. & Kwiat, P. Observation of the spin hall effect of light via weak measurements. *Science* **319**, 787–790 (2008).
- Dixon, P. B., Starling, D. J., Jordan, A. N. & Howell, J. C. Ultrasensitive beam deflection measurement via interferometric weak value amplification. *Phys. Rev. Lett.* **102**, 173601 (2009).
- Starling, D. J., Dixon, P. B., Williams, N. S., Jordan, A. N. & Howell, J. C. Continuous phase amplification with a sagnac interferometer. *Phys. Rev. A* **82**, 011802 (2010).
- Brunner, N. & Simon, C. Measuring small longitudinal phase shifts: weak measurements or standard interferometry? *Phys. Rev. Lett.* **105**, 010405 (2010).
- Huang, J., Li, Y., Fang, C., Li, H. & Zeng, G. Toward ultrahigh sensitivity in weak-value amplification. *Phys. Rev. A* **100**, 012109 (2019).
- Li, H. et al. High-precision temperature measurement based on weak measurement using nematic liquid crystals. *Appl. Phys. Lett.* **112**, 231901 (2018).

31. Li, Y. et al. High-precision temperature sensor based on weak measurement. *Opt. Express* **27**, 21455–21462 (2019).
32. Qiu, X. et al. Precision phase estimation based on weak-value amplification. *Appl. Phys. Lett.* **110**, 071105 (2017).
33. Luo, Z. et al. Low-frequency fiber optic hydrophone based on weak value amplification. *Opt. Express* **28**, 25935–25948 (2020).
34. Song, Q. et al. Adaptive time-varying parameter estimation via weak measurement. *Phys. Rev. Appl.* **18**, 044031 (2022).
35. Song, Q. et al. Surpassing the nyquist sampling limit via postmodulation. *Phys. Rev. Appl.* **18**, 034077 (2022).
36. Li, H. et al. High precision phase estimation with controllable sensitivity and dynamic range. *J. Phys. B: At. Mol. Opt. Phys.* **54**, 215503 (2021).
37. Stupin, D. D., Koniakhin, S. V., Verlov, N. A. & Dubina, M. V. Adaptive filtering to enhance noise immunity of impedance and admittance spectroscopy: Comparison with fourier transformation. *Phys. Rev. Appl.* **7**, 054024 (2017).
38. Eleuteri, A. et al. Adaptive filters for detection of gravitational waves from coalescing binaries. *Phys. Rev. D.* **73**, 122004 (2006).
39. Chassande-Mottin, E. & Dhurandhar, S. V. Adaptive filtering techniques for gravitational wave interferometric data: Removing long-term sinusoidal disturbances and oscillatory transients. *Phys. Rev. D.* **63**, 042004 (2001).
40. Haykin, S. *Adaptive Filter Theory, Fifth Edition* (Publishing House of Electronics Industry, Beijing, 2016).
41. Molisch, A. F. *Wireless Communications, Second Edition* (Publishing House of Electronics Industry, Beijing, 2015).
42. Chen, G. et al. Beating standard quantum limit with weak measurement. *Entropy* **23**, 354 (2021).
43. Huang, J.-Z., Fang, C. & Zeng, G. Weak-value-amplification metrology without spectral analysis. *Phys. Rev. A* **97**, 063853 (2018).
44. Martínez-Rincón, J., Liu, W., Viza, G. I. & Howell, J. C. Can anomalous amplification be attained without postselection? *Phys. Rev. Lett.* **116**, 100803 (2016).
45. Zhang, L., Datta, A. & Walmsley, I. A. Precision metrology using weak measurements. *Phys. Rev. Lett.* **114**, 210801 (2015).
46. Tse, M. E. et al. Quantum-enhanced advanced ligo detectors in the era of gravitational-wave astronomy. *Phys. Rev. Lett.* **123**, 231107 (2019).
47. Aasi, J. et al. Enhanced sensitivity of the ligo gravitational wave detector by using squeezed states of light. *Nat. Photonics* **7**, 613–619 (2013).
48. Monras, A. Optimal phase measurements with pure gaussian states. *Phys. Rev. A* **73**, 033821 (2006).
49. Berni, A. A. et al. Ab initio quantum-enhanced optical phase estimation using real-time feedback control. *Nat. Photonics* **9**, 577–581 (2015).
50. Yu, J. et al. Quantum enhanced optical phase estimation with a squeezed thermal state. *Phys. Rev. Appl.* **13**, 024037 (2020).
51. Ou, Z. Y. Complementarity and fundamental limit in precision phase measurement. *Phys. Rev. Lett.* **77**, 2352–2355 (1996).
52. Ou, Z. Y. Fundamental quantum limit in precision phase measurement. *Phys. Rev. A* **55**, 2598–2609 (1997).
53. Tan, J., Cao, Y., Huang, H. & Guo, H. Modeling and characterization of marine ambient noise in the arctic. *J. Appl. Acoust.* **39**, 690–697 (2020).
54. Ma, J., Ge, L. & Tong, L. New time delay estimation algorithm of hf fading signal in symmetric α -stable distribution noise environments. *J. Signal Process.* **30**, 526–534 (2014).
55. Barone, C. & Pagano, S. What can electric noise spectroscopy tell us on the physics of perovskites? *Coatings* **11**, 96 (2021).
56. Li, F., Huang, J. & Zeng, G. Adaptive weak-value amplification with adjustable postselection. *Phys. Rev. A* **96**, 032112 (2017).
57. Wang, G., Li, H., Xiao, T., Huang, J. & Zeng, G. Adaptive correction of phase estimation with time based on weak measurement. *Opt. Express* **29**, 39150–39158 (2021).

Acknowledgements

This work is supported by the National Natural Science Foundation of China (Grants No.61901258 and No.62071298), and Innovation Program for Quantum Science and Technology (Grants No.2021ZD0300703). In addition, all authors would thank Shurong Wei and Han Wang for their help in setting up the experiment, both of them are from Institute for Quantum Sensing and Information Processing (QSIP) of Shanghai Jiao Tong University.

Author contributions

G.Z. and H.L. conceived the research project, H.L. and Q.S. designed the scheme, Q.S. constructed the theoretical model and carried out the experiments with assistance from H.L., J.H., P.H., X.T. and C.S. Q.S. and H.L. wrote the manuscript with assistance from G.Z., P.H. and Y.T.

Competing interests

The authors declare no competing interests.

Additional information

Correspondence and requests for materials should be addressed to Hongjing Li or Guihua Zeng.

Peer review information *Communications Physics* thanks the anonymous reviewers for their contribution to the peer review of this work.

Reprints and permission information is available at <http://www.nature.com/reprints>

Publisher's note Springer Nature remains neutral with regard to jurisdictional claims in published maps and institutional affiliations.



Open Access This article is licensed under a Creative Commons Attribution 4.0 International License, which permits use, sharing, adaptation, distribution and reproduction in any medium or format, as long as you give appropriate credit to the original author(s) and the source, provide a link to the Creative Commons license, and indicate if changes were made. The images or other third party material in this article are included in the article's Creative Commons license, unless indicated otherwise in a credit line to the material. If material is not included in the article's Creative Commons license and your intended use is not permitted by statutory regulation or exceeds the permitted use, you will need to obtain permission directly from the copyright holder. To view a copy of this license, visit <http://creativecommons.org/licenses/by/4.0/>.

© The Author(s) 2023